



HAL
open science

High-repetition-rate source delivering optical pulse trains with a controllable level of amplitude and temporal jitters

Ugo Andral, Christophe Finot

► **To cite this version:**

Ugo Andral, Christophe Finot. High-repetition-rate source delivering optical pulse trains with a controllable level of amplitude and temporal jitters. *Engineering Reports*, 2020, 2, pp.e12182. 10.1002/eng2.12182 . hal-02332668v2

HAL Id: hal-02332668

<https://hal.science/hal-02332668v2>

Submitted on 18 May 2020

HAL is a multi-disciplinary open access archive for the deposit and dissemination of scientific research documents, whether they are published or not. The documents may come from teaching and research institutions in France or abroad, or from public or private research centers.

L'archive ouverte pluridisciplinaire **HAL**, est destinée au dépôt et à la diffusion de documents scientifiques de niveau recherche, publiés ou non, émanant des établissements d'enseignement et de recherche français ou étrangers, des laboratoires publics ou privés.



High-repetition-rate source delivering optical pulse trains with a controllable level of amplitude and temporal jitters

Ugo Andral | Christophe Finot

Laboratoire Interdisciplinaire CARNOT de Bourgogne, UMR 6303 CNRS-Université de Bourgogne-Franche Comté, Dijon, France

Correspondence

Christophe Finot, Université de Bourgogne-Franche Comté, 9 av. Alain Savary, 21 000 Dijon, France.
Email: christophe.finot@u-bourgogne.fr

Funding information

Agence Nationale de la Recherche, Grant/Award Number: ANR-11-LABX-01-01; French Investissements d'Avenir program; the Bourgogne-Franche Comté Region; Institut Universitaire de France (IUF)

Abstract

We theoretically propose and numerically validate an all-optical scheme to generate optical pulse trains with varying peak-powers and durations. A shaping of the spectral phase thanks to discrete $\pi/2$ phase shifts enables an efficient phase-to-intensity conversion of a temporal phase modulation based on a two-tone sinusoidal beating. Experiments carried out at telecommunication wavelengths and at a repetition rate of 10 GHz confirm the ability of our approach to efficiently generate a train made of pulses with properties that vary from pulse-to-pulse. The levels of jitters can be accurately controlled.

KEYWORDS

high-repetition rate optical pulse trains, optical component testing, optical telecommunications

1 | INTRODUCTION

The generation of pulse trains at repetition rates of several tens of GHz remains a crucial step for the testing of optical components. In order to assess the performance of devices under realistic conditions, it is relevant to have a source which quality can be adjusted to mimic the presence of various kinds of degradations that may impair the optical function under test. Whereas the optical signal-to-noise ratio can be straightforwardly adjusted using an external source of amplified spontaneous emission, jitters of the peak-power, and duration of the pulses are more challenging to control, especially when these fluctuations are on a short time scale and affect pulses with a low duty cycle. Indeed, the current bandwidth limitations of optoelectronic devices do not allow the direct generation of picosecond pulses directly from intensity modulators. As a consequence, alternate solutions are required to generate the pulse train such as actively mode-locked fiber lasers¹ or cavity-free techniques based on the nonlinear reshaping of a sinusoidal beating.^{2,3} These approaches have in common a very high stability and the resulting pulses are perfectly defined without any fluctuations of their temporal profile, which may limit their use for component testing applications. Another attractive solution is based on a direct temporal phase modulation that is then converted into an intensity modulation thanks to a quadratic spectral phase.^{4,5} Picosecond pulses at repetition rates of several tens of GHz have been successfully demonstrated and such a source can be involved in optical sampling.⁶ However, this approach suffers from a limited extinction ratio and from the presence of detrimental temporal sidelobes,⁷ so that a considerable part of the energy lies outside the main pulse. By replacing the quadratic spectral phase modulation by a triangular one, we have recently shown that

This is an open access article under the terms of the Creative Commons Attribution License, which permits use, distribution and reproduction in any medium, provided the original work is properly cited.

© 2020 The Authors. *Engineering Reports* published by John Wiley & Sons, Ltd.

it was possible to generate Fourier-transform limited, close-to-Gaussian pulses⁸ that are well suited for return-to-zero transmissions.

We extend here theoretically and experimentally this scheme and we demonstrate that an architecture based on a dual tone sinusoidal phase modulation can efficiently sustain the generation of a train of pulses with peak-powers and durations that vary from pulse-to-pulse. The rate of change as well as the level of fluctuations can be easily controlled in a periodic and deterministic way by adjusting the RF properties of the second tone.

Our article is therefore organized as follows. We first describe the principle of our approach before assessing by numerical simulations and by an approximate analytical model the ultrafast fluctuations that are imprinted on the pulse train. We then validate our optical architecture experimentally for a pulse train at a repetition rate of 10 GHz.

2 | PRINCIPLE OF OPERATION AND NUMERICAL SIMULATIONS

2.1 | Pulse generation process

Before explaining our approach, let us first recall the basis of the generation of a stable pulse train from a temporal sinusoidal phase modulation as recently introduced in Reference 8. We consider a continuous optical wave with a power P_0 and an optical carrier frequency ω_c , $\Psi(t) = \sqrt{P_0} \psi(t) e^{i\omega_c t}$, which phase is temporally modulated by a sinusoidal waveform $\varphi(t)$:

$$\begin{cases} \psi(t) = e^{i \varphi(t)} \\ \varphi(t) = A_m \cos(\omega_m t) \end{cases}, \quad (1)$$

where A_m is the amplitude of the phase modulation and ω_m its angular frequency. The temporal sinusoidal phase leads to a set of spectral lines that are equally spaced by ω_m and which amplitude can be expressed using a Jacobi-Anger expansion^{9,10}:

$$\psi(t) = \sum_{n=-\infty}^{\infty} i^n J_n(A_m) e^{in\omega_m t}, \quad (2)$$

with J_n being the Bessel function of the first kind of order n . An essential point is the existence of a phase shift of $\pi/2$ between each spectral component. With the progress of linear shaping, one can now process a line-by-line spectral phase profile using liquid-crystal modulators¹¹ or fiber Bragg gratings.¹² It then becomes feasible to imprint an exact spectral phase profile of opposite sign. Quite remarkably, this spectral phase profile to be applied in order to obtain a flat spectral phase does not depend on the value of A_m . The resulting temporal profile is a Fourier-transform limited waveform $\psi'(t)$ at a repetition rate $f_m = \omega_m/2\pi$ (leading to a period $T_0 = 1/f_m$) that has been called a *besselon wave*¹³ and can be analytically expressed as:

$$\psi'(t) = J_0(A_m) + 2 \sum_{n=1}^{\infty} J_n(A_m) \cos(n\omega_m t). \quad (3)$$

We have reported in Figure 1A the resulting intensity profiles that are obtained for various values of A_m . According to the amplitude of the initial temporal phase modulation A_m , the temporal duration, the peak-power and the overall pulse shape vary significantly. However, as the phase-to-intensity conversion process is not dissipative, let us note that all the waveforms have the same energy over a period T_0 . The value $A_m = 1.1$ rad (Figure 1A2) is of high interest as a clean Gaussian-like structure is achieved, with a high extinction ratio.⁸ For lower values such as $A_m = 0.6$ rad (Figure 1A1), a residual background is visible and the shape is close to an Akhmediev breather.¹⁴ For values of A_m higher than 1.1 rad (Figure 1A3), the extinction ratio is decreased but shorter durations and higher peak-powers can be reached.¹³ The detailed evolutions of the peak-power and of the full-width at half maximum (fwhm) duration are provided in Figure 1B,C. We note that these quantities evolve monotonously and that they can vary over a factor above 4. Around $A_m = 1.1$ rad, it is possible to approximate their evolutions by linear fits (dashed gray lines).

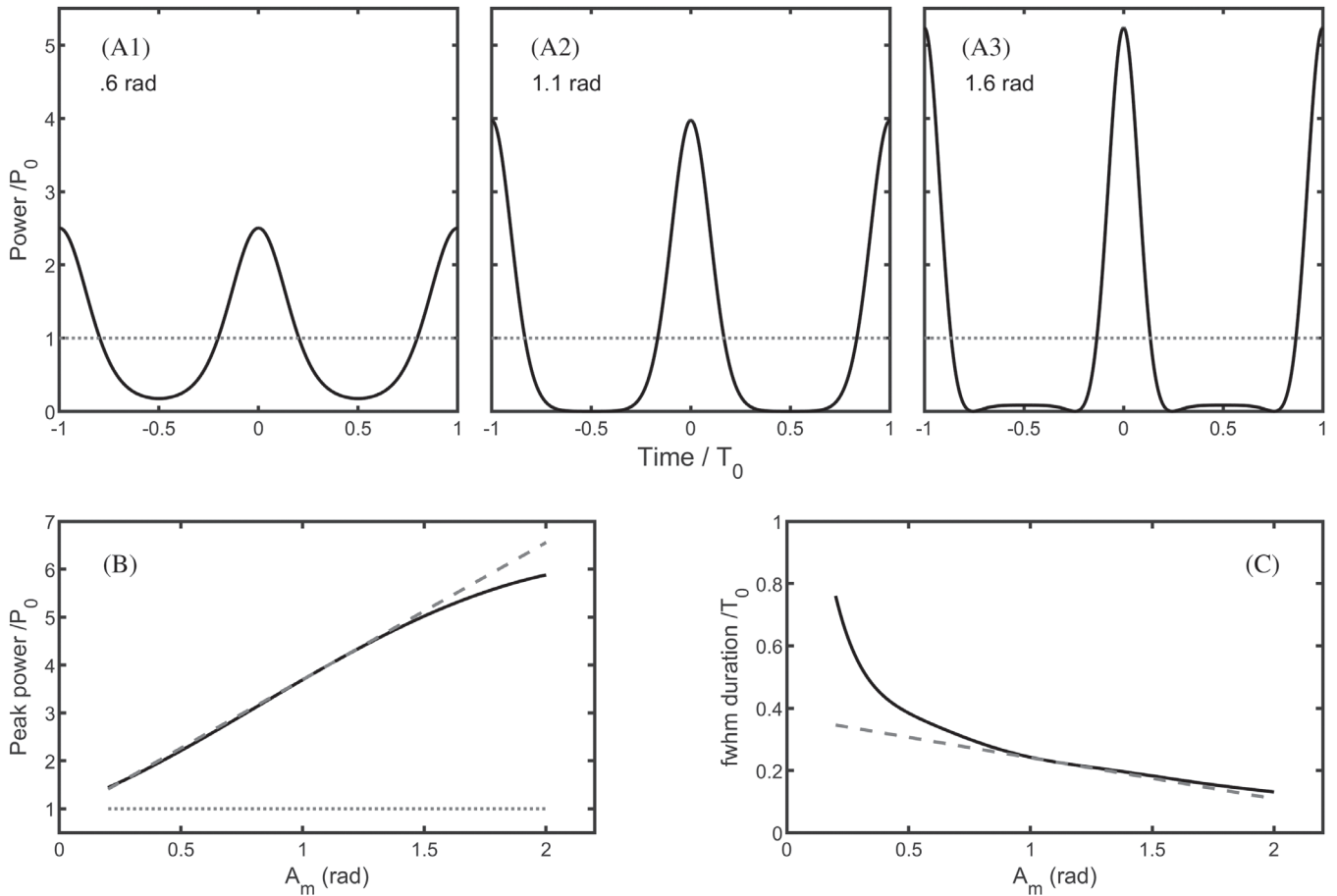


Figure 1 (A) Temporal intensity profiles obtained for different amplitude of phase modulation ($A_m = 0.6, 1.1,$ and 1.6 rad, panels 1, 2, and 3 respectively). Evolutions of the peak-power and of the temporal duration of the resulting structure (panels B and C, respectively). Results of numerical simulations (solid black lines) are compared with a first-order Taylor expansion around $A_m = 1.1$ rad (dashed gray line). The gray dotted lines are for the temporal intensity profiles obtained before the $\pi/2$ spectral phase shifts

2.2 | Ultrafast modulation of the pulse properties

Let us now describe our approach to generate a pulse train with properties varying from pulse-to-pulse. We replace the sinusoidal phase modulation used in (1) by a two-tone temporal phase modulation:

$$\varphi'(t) = A_1 \cos(\omega_1 t) + A_2 \cos(\omega_2 t), \quad (4)$$

where A_1 and A_2 are the amplitude of the sinusoidal phase modulation at angular frequencies ω_1 and $\omega_2 = \omega_1 + \Delta\omega$, respectively. Combining these two sinusoidal modulations induces a beating characterized by fast oscillations with a frequency ω'_m (leading to a period T'_0) and by a slow envelope with a frequency ω_b (leading to a period T_b). Typical examples of these temporal beatings are plotted on Figure 2A. The resulting optical spectrum (Figure 2B1) involves a set of spectral lines with typical spaces $\Delta\omega$ and ω_1 . The spectral shaping based on discrete $\pi/2$ phase shifts (Figure 2B2) can efficiently be applied to each subset of spectral lines. As a consequence, we can expect that over the time scale of a fast temporal oscillation T'_0 , the phase-to-intensity conversion will be qualitatively as efficient as the one obtained based on a purely sinusoidal modulation with an amplitude A'_m provided by the envelope of the beating:

$$A'_m(t) = \sqrt{A_1^2 + A_2^2 + 2 A_1 A_2 \cos(\Delta\omega t)}. \quad (5)$$

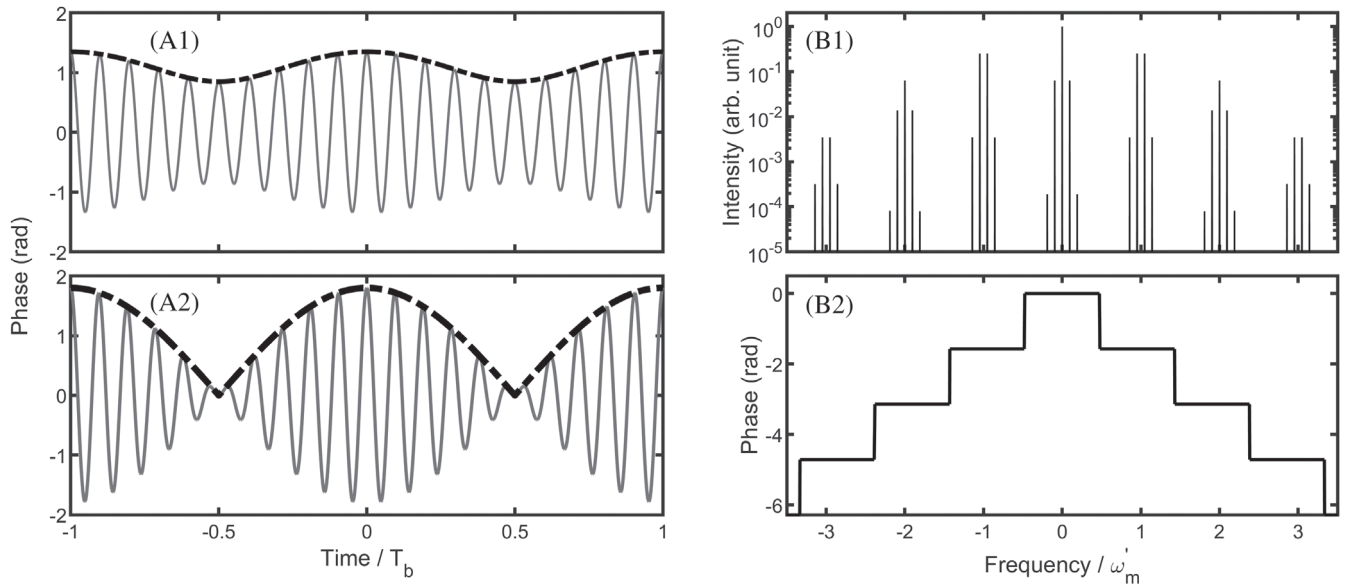


Figure 2 (A) Temporal phase profiles resulting from the superposition of two sinusoidal phase modulation (gray solid line). Numerical results obtained for $A_1 = 1.1$ rad and $A_2 = 0.25$ rad (panel A1) or for $A_1 = 0.9$ rad and $A_2 = 0.9$ rad (panel A2). $\Delta\omega = 0.1 \omega_1$. Envelope predicted by Equations (6) and (8) are plotted with black mixed line. (B1) Optical spectrum obtained for $A_1 = A_2$. (B2) Spectral phase mask applied to the signal

In order to get better understanding, it is interesting to discuss two limiting cases. When $A_1 \gg A_2$ (see for example panel A1 of Figure 2), the envelope of the phase modulation can be approximated by a sinusoidal modulation (black mixed line):

$$A'_m(t) \simeq A_1 + A_2 \cos(\Delta\omega t). \quad (6)$$

When $A_1 = 1.1$ rad, one can benefit from the linear approximation used in Figure 1B: the peak-power of the resulting pulses is impacted by the beating and will also follow a sinusoidal variation (see Figure 3A, black mixed line), which amplitude is directly controlled by A_2 . Pulse duration also changes, but for moderate values of A_2 , the overall shape remains close to a Gaussian waveform. Similar qualitative conclusions can be drawn for other amplitudes of A_2 as illustrated in panels (C) and (D) of Figure 3 obtained for $A_2 = 0.1$ and 0.5 rad, respectively.

Another interesting case is when $A_1 = A_2$ (see Figure 2A2). In this well-known case in wave physics,^{15,16} Equation (4) can be rewritten as:

$$\varphi'(t) = 2 A_1 \cos\left(\frac{\Delta\omega}{2} t\right) \cos\left(\frac{\omega_2 + \omega_1}{2} t\right), \quad (7)$$

leading to

$$A'_m(t) \simeq 2A_1 |\cos(\Delta\omega t)| \quad (8)$$

The fast oscillations have a frequency $\omega'_m = (\omega_1 + \omega_2)/2$. The envelope is modulated between 0 and $2 A_1$ at an angular frequency $\Delta\omega$. This results in rapidly varying pulses, with amplitude, duration, shape, and extinction ratio experiencing major changes (see Figure 3B).

2.3 | Performance assessment

In order to more quantitatively assess the ultrafast changes of the various properties experienced by the pulses, we have reported in Figure 4, the temporal evolution of the peak-power, of the extinction ratio and of the duration. Results are

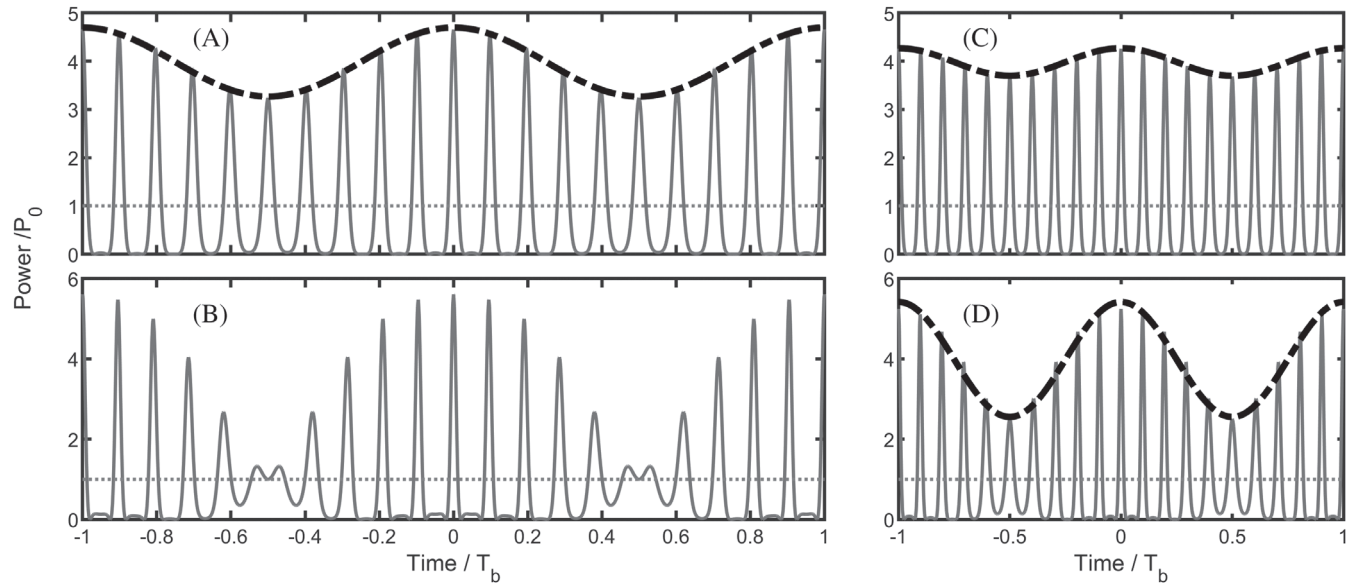


Figure 3 Temporal intensity profiles resulting from the superposition of two temporal sinusoidal phase modulations after triangular spectral processing. Numerical results (gray line) are obtained at $\Delta\omega = 0.1 \omega_1$ for $A_1 = 1.1$ rad and $A_2 = 0.25$ rad (panel A), for $A_1 = 0.9$ rad and $A_2 = 0.9$ rad (panel B), for $A_1 = 1.1$ rad and $A_2 = 0.1$ rad (panel C), for $A_1 = 1.1$ rad and $A_2 = 0.5$ rad (panel D). Black mixed line represents the fluctuations of the peak-power based on Equation (6) and the linear approximation from Figure 1B. The dotted gray lines represent the temporal intensity profile before the $\pi/2$ spectral phase shifts

evaluated over each period T'_0 ($\Delta\omega$ being fixed here to $0.01 \omega_1$) for different combinations of A_1 and A_2 . The kurtosis excess (computed over the central part of the pulse, that is, between two minima) also enables us to stress the changes in the temporal intensity profiles.¹⁷ From Figure 4, one can first note that for operation around A_1 fixed to 1.1 rad, the impact of the changes is directly linked to the amplitude of A_2 . Whereas only moderate modulations are expected for $A_2 = 0.1$ rad, increasing A_2 to 0.5 rad significantly increases the range of fluctuations of the peak-power and durations, with peak-power that can vary by a factor of 2. The extinction ratio is also affected and some waveforms have an extinction ratio as poor as 10 dB. With fluctuations of the Kurtosis excess between -0.15 and 0.7 , the temporal profile of each pulse can also be affected. When $A_1 = A_2 = 0.9$ rad, the range of the fluctuations is dramatically increased, with some waveforms presenting very low extinction ratios, indicating the presence of a strong continuous and coherent background for some pulses.

We have also compared in Figure 4 the changes in the various parameters achieved with our two-tone temporal phase modulation ($A_2 = 1.1$ rad and $A_2 = 0.25$ rad) and the results achieved by a cascading phase modulator, a spectral phase shaper and an intensity modulator leading to the same depth of peak-power fluctuations (open circles). This outlines that, contrary to our proposed scheme, the scheme based on cascading phase and intensity modulators only induces fluctuations of the peak power and does not have any impact on the overall pulse waveform.

We summarized in Figure 5 the evolution according to A_2 for $A_1 = 1.1$ rad of the amplitudes of fluctuation ΔP , $\Delta T_{1/2}$, and ΔE of the peak-power, the fwhm duration and the pulse energy respectively normalized to their average value. ΔP , $\Delta T_{1/2}$, and ΔE are here defined as the difference between the maximal and minimal values that are recorded during the beating period T_b . We can note that ΔP and $\Delta T_{1/2}$ evolve monotonously with A_2 . For A_2 below 0.3 rad, the evolution obtained from numerical simulations follows closely a linear trend and can be predicted from the linear fits applied in panels (B) and (C) of Figure 1. As a consequence, the level of jitters applied to the waveform is easily controlled. Regarding ΔE , Figure 5C stresses that the fluctuations of the pulse energy are extremely reduced (below 2%), further confirming that our process strongly differs from a simple intensity modulation of the envelope of the pulse train.

For $A_2 = 0.5$ rad, the range of fluctuations of the peak-power and the duration of the pulses can be as high as 67% of the average values. This leads to a major modification of the eye diagrams as stressed in Figure 6. For moderate values of A_2 (panel A of Figure 6), the eye remains clearly open, but with noticeable amplitude jitter. The probability distribution function of the peak-power exhibits a shape that is typical of sinusoidal fluctuations, as already measured for example in

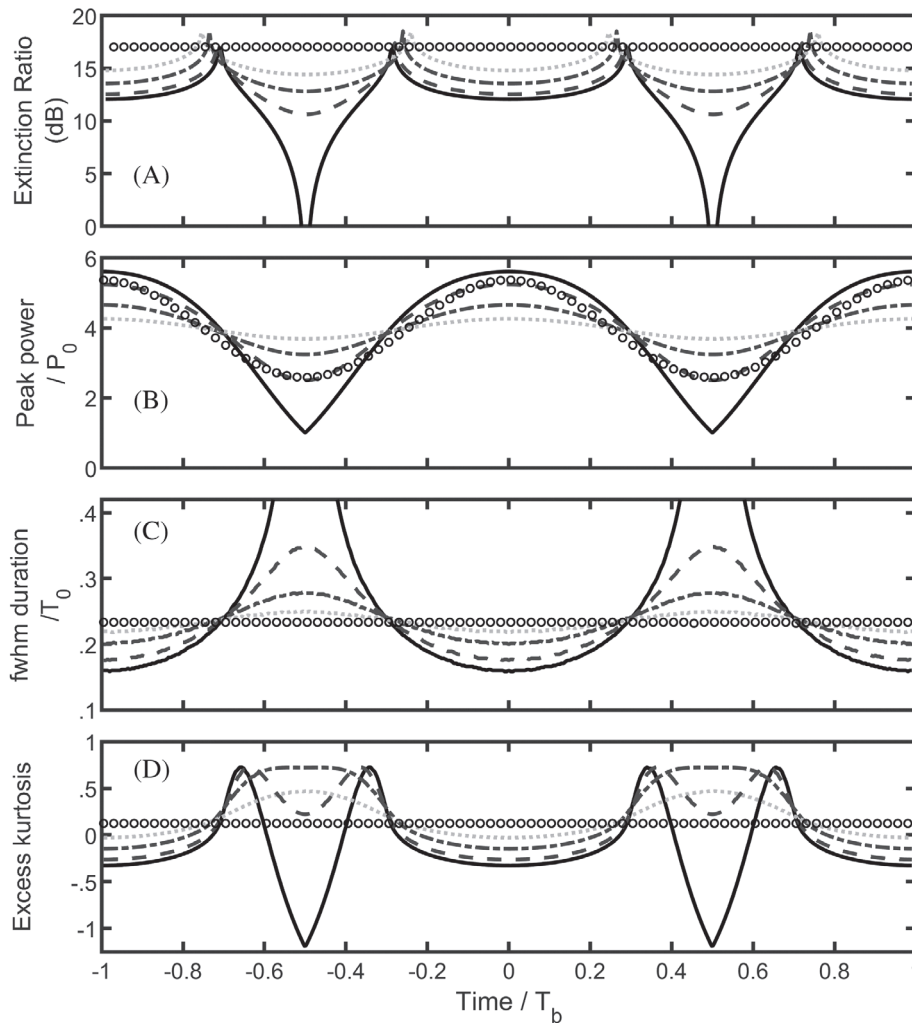


Figure 4 Temporal evolution of different parameters for various combinations of parameters (A_1, A_2): (1.1, 0.1) (light gray dotted line); (1.1, 0.25) (gray mixed line); (1.1, 0.5) (dark gray dashed line); (0.9, 0.9) (black solid line). Evolution of the extinction ratio, of the peak-power, of the fwhm duration and of kurtosis excess (panels A, B, C, and D, respectively). Results obtained for $\Delta\omega = 0.01 \omega_1$. The dotted open circles are the results obtained from the cascading of a first stage of spectrally processed single-tone temporal phase modulation followed by an intensity modulation at $\Delta\omega$ with a modulation depth similar to the results achieved with $A_1 = 1.1$ and $A_2 = 0.25$

the past using jitter magnifiers.¹⁸ For $A_2 = 0.5$ rad (panel B), both the amplitude jitter and the changes in the temporal duration contribute to the closure of the eye diagram. For a configuration where A_2 and A_1 are balanced (panel C), the level of fluctuations is greatly increased and the eye closed. The poor extinction ratio is also readily visible on the eye diagram.

3 | EXPERIMENTAL VALIDATION

3.1 | Experimental setup

The experimental setup is sketched on Figure 7 and is based on devices that are commercially available and typical of the telecommunication industry. An external cavity laser delivers a continuous wave at 1550 nm that is then temporally phase modulated using two Lithium Niobate electro-optic devices (iXblue MPZ-LN-20) driven by sinusoidal electrical signals at frequencies ω_1 and ω_2 . The optical phase modulations have an amplitude A_1 and A_2 . Note that a single phase modulator could be used if the electrical sinusoidal waveforms can be mixed in the electrical domain. For these proof-of-principle experiments, ω_1 has been fixed to 10 GHz. A linear spectral shaper (Finisar Waveshaper 1000A) based on liquid crystal on silicon technology¹⁹ is then used to apply the discrete spectral phase shifts of $\pi/2$ between two successive components. Our setup is fully fibered and in order to ensure enhanced environmental stability, polarization-maintaining components have been used. Moreover, since the principle of operation is purely linear, no Erbium doped fiber amplifier is required, thus limiting the source of detrimental noise. The reshaping process is energy efficient, since the optical losses are restricted to the insertion losses of the phase modulators (2×2 dB) and of the spectral shaper (4 dB). This 8-dB losses are lower than what could be achieved using cascaded intensity modulators, that, in addition to the optical losses, remove a significant part of the signal energy.

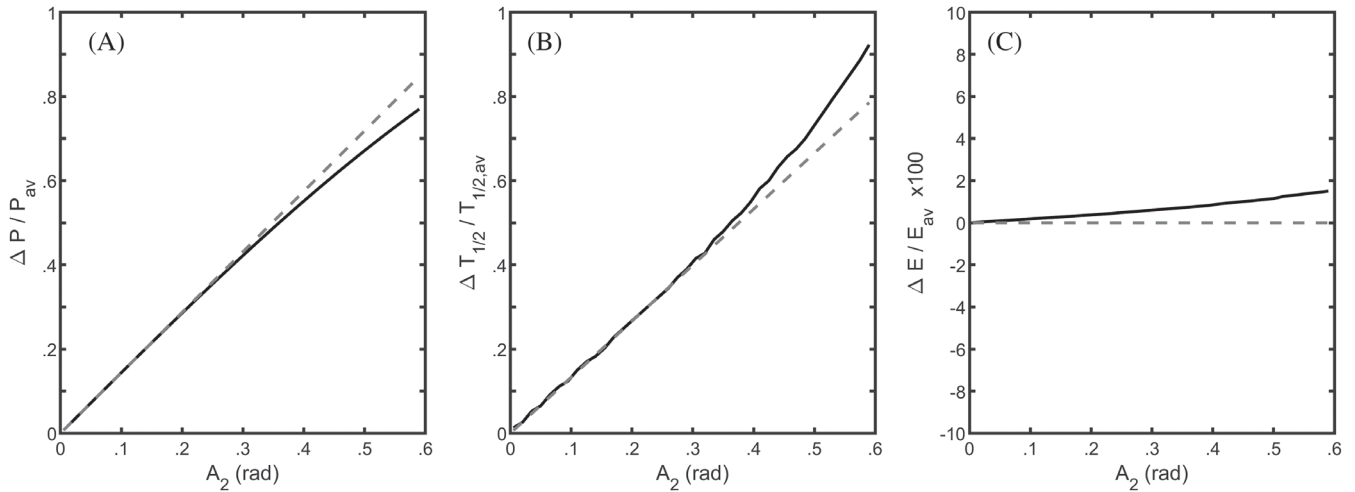


Figure 5 Evolution of the amplitude jitter, the temporal width jitter and the energy jitter (panels A, B, and C respectively) according to the level of phase modulation A_2 for a fixed value of $A_1 = 1.1$ rad. Results of numerical simulations (solid black lines) are compared with a linear trend based on the linear fits applied in Figure 1B,C

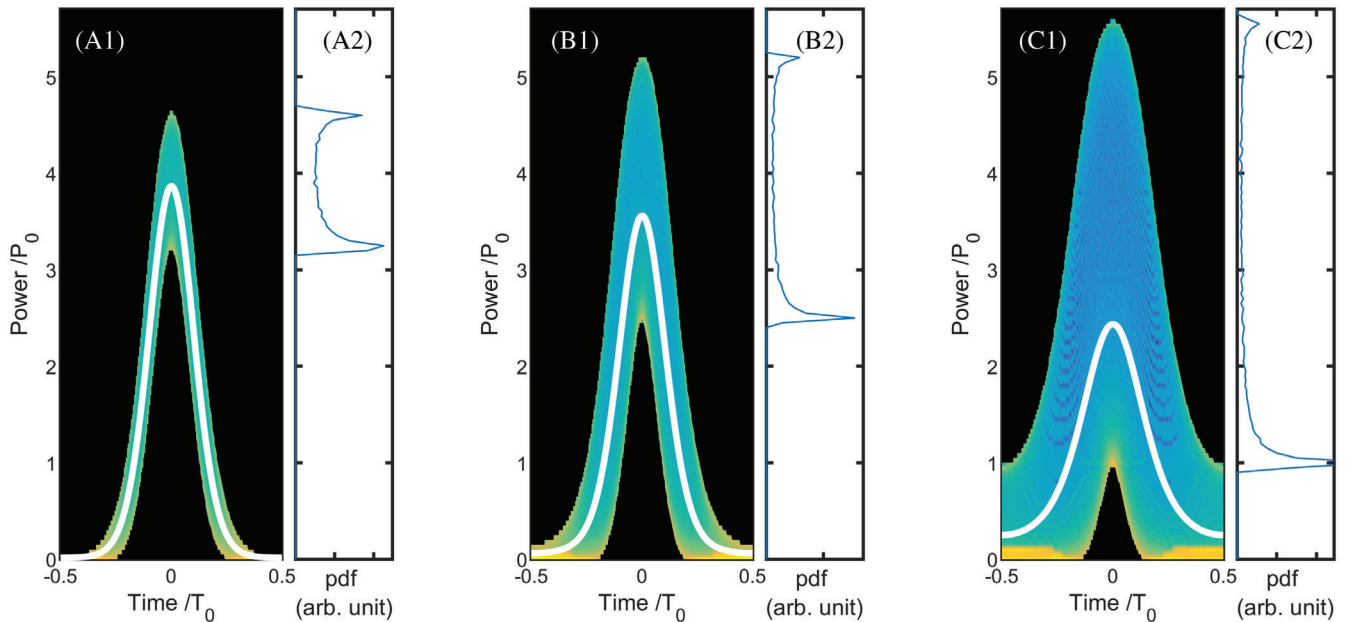


Figure 6 Eye diagrams and probability distribution function (pdf) of the peak-power of the pulse (panels 1 and 2, respectively) recorded for different combinations of phase parameters (A_1, A_2) : (1.1, 0.25) (panel A); (1.1, 0.5) (panel B); (0.9, 0.9) (panel C). Results obtained for $\Delta\omega = 0.01 \omega_1$. The white line represents the waveform obtained from averaging

The resulting signal is directly recorded by means of a high-speed optical sampling oscilloscope (1 ps resolution, EXFO PSO 101), an electrical sampling oscilloscope (50 GHz bandwidth) and a high-resolution optical spectrum analyser (5 MHz resolution, APEX AP207).

3.2 | Experimental results

In order to validate our concept, we have first recorded the temporal waveforms that are generated when temporal phase modulations have frequencies of $\omega_1 = 10$ GHz and $\omega_2 = 11$ GHz, associated with an amplitude of modulation of

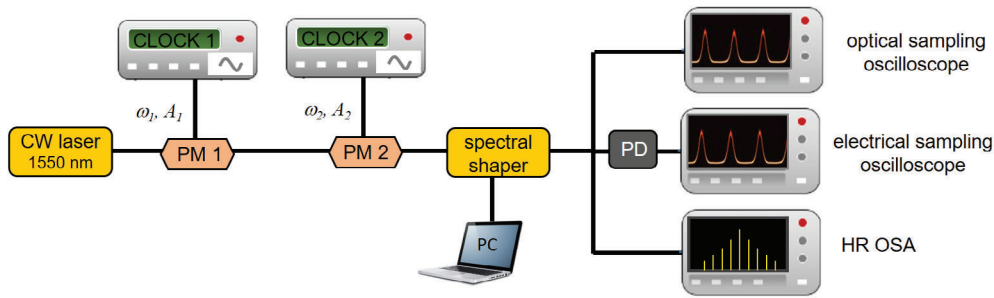


Figure 7 Experimental setup. CW, continuous wave; PM, phase modulator; HR OSA, high resolution optical spectrum analyser; PD, Photodiode

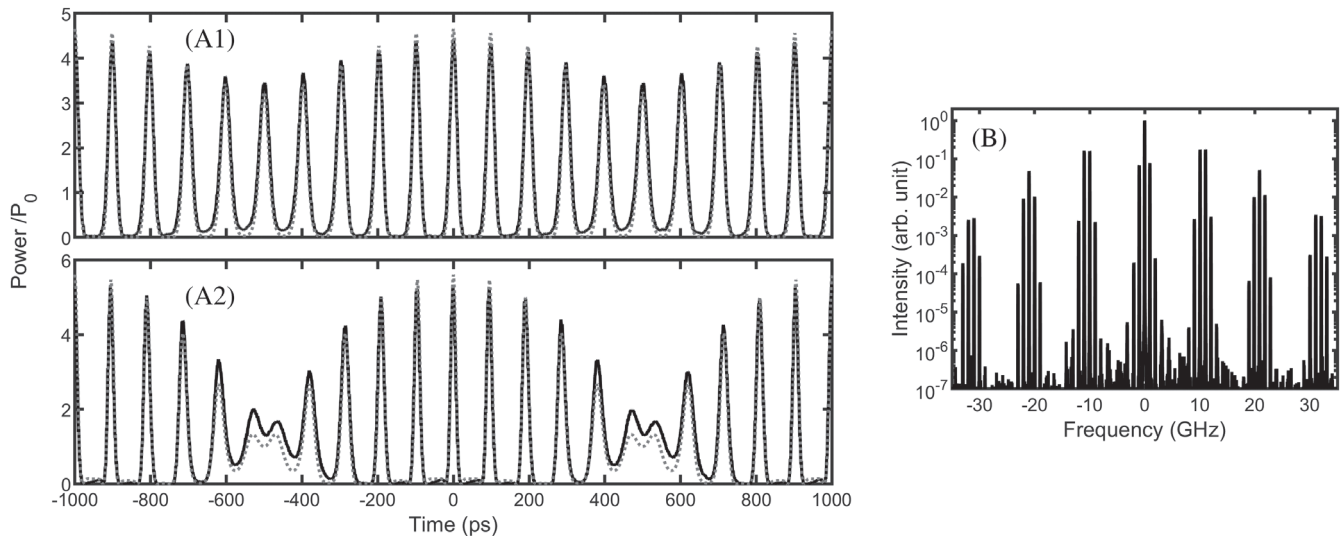


Figure 8 (A) Temporal intensity profiles resulting from the superposition of two sinusoidal phase modulation and spectral processing. Results obtained for $A_1 = 1.1$ rad and $A_2 = 0.25$ rad (panel A1) or for $A_1 = 0.9$ rad and $A_2 = 0.9$ rad (panel A2). Experimental results recorded on the optical sampling oscilloscope (solid black line) are compared with numerical simulations (gray dotted lines) (B) Optical spectrum recorded for $A_1 = 0.9$ rad and $A_2 = 0.9$ rad. All results are recorded for $\omega_1 = 10$ GHz and $\omega_2 = 11$ GHz

$A_1 = 1.1$ rad and $A_2 = 0.25$ rad (panel A1) or $A_1 = A_2 = 0.9$ rad (panel A2). Results are recorded on an optical sampling oscilloscope and plotted on Figure 8A. The experimental waveforms outline that modification of the temporal pulse properties on a pulse-to-pulse basis is efficiently achieved: in both cases, each pulse of the 10 pulses sequence exhibits features that are different from its nearest neighbor. Changes in the peak-power are associated with changes of the temporal duration and the residual background can also vary. The excellent agreement that is obtained with the numerical simulations (see dotted gray line) stresses the accurate control that can be achieved by simply adjusting the amplitude of the phase modulation. The typical optical spectrum as shown in panel (B) of Figure 8 confirms the high level of the optical signal to noise ratio, stressing that the observed fluctuations are fully deterministic and cannot be linked to any amplified spontaneous emission.

We performed additional measurements using a longer sequence of modulated pulses (ie, with $\omega_1 = 10$ GHz and $\omega_2 = 10.1$ GHz) for a fixed value of $A_1 = 1.1$ rad and values of A_2 spanning from 0.1 rad to 0.6 rad. Benefiting from the electrical sampling oscilloscope, we were able to record the resulting 10 ns pulse train. Summary of the fluctuation levels of the peak-power, the temporal duration and the pulse energy is presented in Figure 9. Fluctuations of the peak-power and of the duration increase with the amplitude of A_2 . On the contrary, the pulse energy is not heavily impacted by A_2 , with fluctuations well below 10% that are consistent with our theoretical expectations. All the experimental trends qualitatively reproduce the numerical results described in Figure 5. The deviation that is observed can be mainly ascribed to the finite bandwidth of our optoelectronic detection.

As a final measurement, we reconstructed eye diagrams from the experimental measurements. Results are provided on Figure 10 for three different levels of jitters, corresponding to $A_2 = 0.25$ rad or 1.5 rad with A_1 being fixed to 1.1 rad (panels A and B respectively), or to $A_2 = A_1 = 0.9$ rad (panel C). Once again, the experimental results are found in qualitative

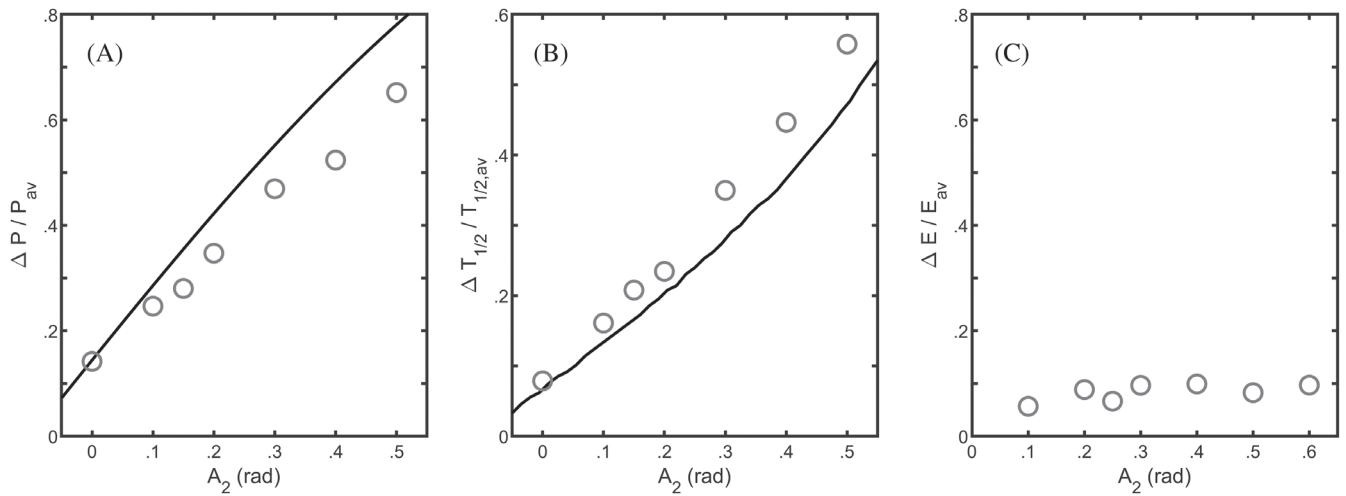


Figure 9 Evolution of the amplitude jitter, of the temporal width jitter, and of the energy (panels A, B, and C respectively) according to the level of phase modulation A_2 for a fixed value of $A_1 = 1.1$ rad. Results of numerical simulations (solid black lines) are compared with the experimental results measured on the digital sampling oscilloscope (circles) for $\omega_1 = 10$ GHz and $\Delta\omega = 0.1$ GHz

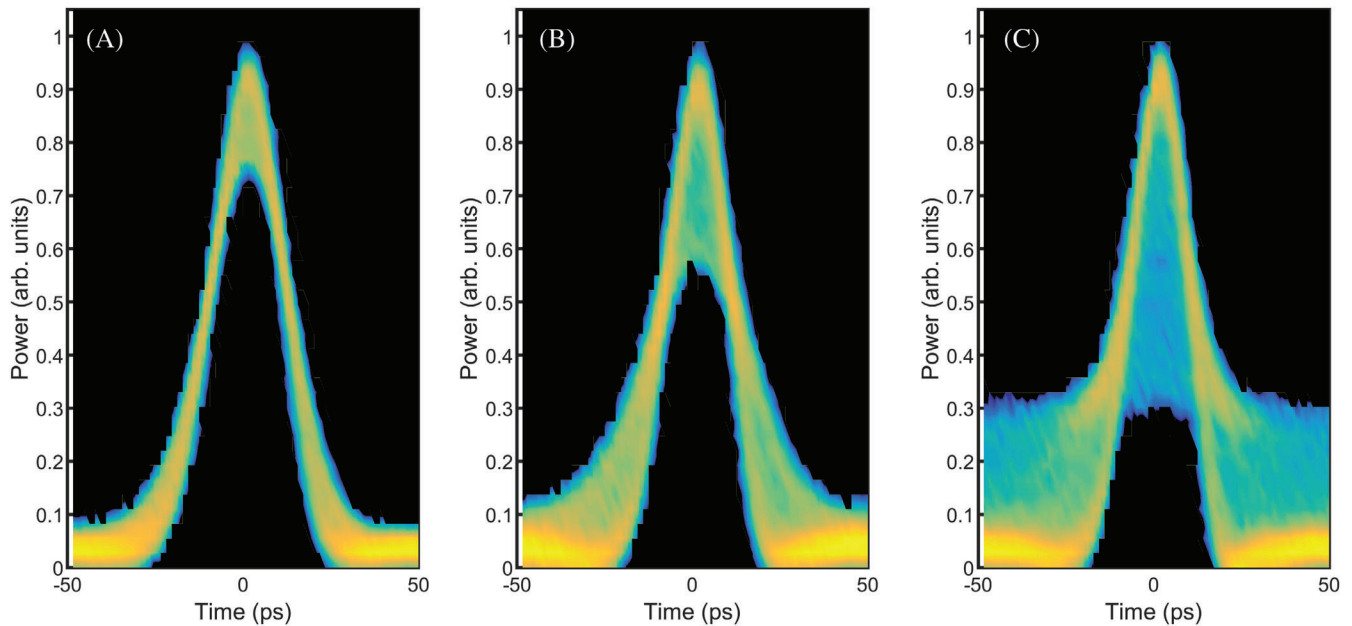


Figure 10 Experimental eye-diagrams recorded for different combinations of phase parameters (A_1, A_2): (1.1, 0.25) (panel A); (1.1, 0.5) (panel B); (0.9, 0.9) (panel C). Results obtained for $\Delta\omega = 0.01 \omega_1$

agreement with the numerical simulations presented in Figure 6. They therefore confirm the various predictions regarding the different regimes that can be observed, ranging from slight fluctuations of the temporal width and peak-power to strong distortions of the temporal properties of the generated waveform.

4 | CONCLUSIONS

In order to conclude, we have theoretically proposed and numerically validated an all-optical scheme to generate optical pulse trains with peak-powers and durations that may significantly vary from pulse-to-pulse, while keeping a pulse energy constant. Our approach relies on a shaping of the spectral phase with $\pi/2$ phase shifts. This enables an efficient phase-to-intensity conversion of a temporal phase modulation based on a two-tone sinusoidal beating. Experiments

fully confirm the ability of our approach to efficiently generate a train made of pulses with properties that vary from pulse-to-pulse in a periodic and deterministic way. The levels of jitters can be accurately controlled and significant levels of fluctuations can be recorded.

Our proof-of-principle experiments have been carried out at a repetition rate of 10 GHz. However, as the principle of a stable pulse train generation has also been validated at 40 GHz,⁸ we expect that similar results and jitters can be reproduced at 40 GHz. As suggested in Reference 20, our approach should also be suitable for multi-wavelength operation. In the present work, we have involved two purely sinusoidal phase modulations. By taking advantage of one frequency-swept sinusoidal wave, it could also be possible to introduce a controlled fluctuation of the temporal position of the pulse.²¹ In order to bring some randomness in the observed jitter, some additional narrow-band filtered noise could be added on the initial electrical signal that drives the phase modulator. The impact of such additional noise will be the subject of future theoretical and experimental investigations to understand the statistical properties of the resulting jitters. We have here mainly focused on the results achieved around the modulation depth of the phase amplitude of the first tone A_1 around 1.1 rad. Recent results have stressed that a second operating point ($A'_1 = 2.86$ rad) could also be suitable to generate shorter pulse structures provided the inclusion of an additional π phase shift on the central spectral component.¹³ An in-depth comparison of the performance achieved at the two operating points also deserves a dedicated study.

ACKNOWLEDGEMENTS

We acknowledge the support of the Institut Universitaire de France (IUF), the Bourgogne-Franche Comté Region, the French Investissements d'Avenir program, and the Agence Nationale de la Recherche (ANR-11-LABX-01-01). We thank Anastasiia Sheveleva, Julien Fatome, and Bertrand Kibler for fruitful discussions or technical help, as well as Kamal Hammani for initial comments. The article has benefited from the PICASSO experimental platform of the University of Burgundy.

PEER REVIEW INFORMATION

Engineering Reports thanks Carlos A. Ríos Ocampo and other anonymous reviewers for their contribution to the peer review of this work.

CONFLICT OF INTEREST

The authors declare no potential conflict of interest.

AUTHOR CONTRIBUTIONS

Christophe Finot contributed to the conceptualization, formal analysis, funding acquisition, project administration, supervision, and writing the original draft. Ugo Andral contributed to the investigation.

ORCID

Christophe Finot  <https://orcid.org/0000-0002-0755-5995>

REFERENCES

1. Carruthers TF, Duling IN. 10-GHz, 1.3-ps erbium fiber laser employing soliton pulse shortening. *Opt Lett*. 1996;21:1927-1929.
2. Inoue T, Namiki S. Pulse compression techniques using highly nonlinear fibers. *Laser Photonics Rev*. 2008;2:83-99.
3. Pitois S, Finot C, Fatome J, Millot G. Generation of 20-GHz picosecond pulse trains in the normal and anomalous dispersion regimes of optical fibers. *Opt Commun*. 2006;260:301-306.
4. Kobayashi T, Yao H, Amano K, Fukushima Y, Morimoto A, Sueta T. Optical pulse compression using high-frequency electrooptic phase modulation. *IEEE J Quantum Electr*. 1988;24:382-387.
5. Komukai T, Yamamoto Y, Kawanishi S. Optical pulse generator using phase modulator and linearly chirped fiber Bragg gratings. *IEEE Photon Technol Lett*. 2005;17:1746-1748.
6. Nuno J, Finot C, Fatome J. Linear sampling and magnification technique based on phase modulators and dispersive elements: the temporal lenticular lens. *Opt Fiber Technol*. 2017;36:125-129.
7. Torres-Company V, Lancis J, Andrés P. Unified approach to describe optical pulse generation by propagation of periodically phase-modulated CW laser light. *Opt Exp*. 2006;14:3171-3180.
8. Andral U, Fatome J, Kibler B, Finot C. Triangular spectral phase tailoring for the generation of high-quality picosecond pulse trains. *Opt Lett*. 2019;44:4913-4916.
9. Abramowitz M, Stegun IA. *Handbook of Mathematical Functions: With Formulas, Graphs, and Mathematical Tables*. Courier Corporation; 1964.

10. Hammani K, Fatome J, Finot C. Applications of sinusoidal phase modulation in temporal optics to highlight some properties of the Fourier transform. *Eur J Phys*. 2019;40:055301.
11. Jiang Z, Leaird DE, Weiner AM. Optical processing based on spectral line-by-line pulse shaping on a phase-modulated CW laser. *IEEE J Quantum Electron*. 2006;42:657-665.
12. Berger NK, Levit B, Fischer B. Reshaping periodic light pulses using cascaded uniform fiber Bragg gratings. *J Lightw Technol*. 2006;24:2746-2751.
13. Sheveleva A, Andral U, Kibler B, Boscolo S, Finot C. Temporal optical Bessel waves for high-repetition rate picosecond sources; 2020. arXiv:2003.12630.
14. Andral U, Kibler B, Dudley JM, Finot C. Akhmediev breather signatures from dispersive propagation of a periodically phase-modulated continuous wave. *Wave Motion*. 2020;95:1025-1045.
15. Hecht E. Optics, 4th, International edition. *Addison-Wesley Series in Physics*. Reading, MA: San Francisco; 2002.
16. Crawford F. Waves: Berkeley physics course. Vol 3.
17. DeCarlo LT. On the meaning and use of kurtosis. *Psychol Methods*. 1997;2:292-307.
18. Finot C, Fatome J. All-optical fiber-based ultrafast amplitude jitter magnifier. *Opt Exp*. 2010;18:18697-18702.
19. Roelens MAF, Frisken S, Bolger J, et al. Dispersion trimming in a reconfigurable wavelength selective switch. *J Lightw Technol*. 2008;26:73-78.
20. Andral U, Finot C. Multiwavelength high-repetition rate source. *Laser Phys*. 2020;30:016203.
21. Finot C. Frequency-swept high-repetition rate optical source. *Microw Opt Technol Lett*. 2020. <https://doi.org/10.1002/mop.32387>.

How to cite this article: Andral U, Finot C. High-repetition-rate source delivering optical pulse trains with a controllable level of amplitude and temporal jitters. *Engineering Reports*. 2020;e12182. <https://doi.org/10.1002/eng2.12182>